Heat transfer in Microchannels

SLAC National Accelerator Laboratory

Giovanni Leonardo Pirozzi

Supervisor: Dr. Marco Oriunno

September 23, 2014

Abstract

Pressure drop and Heat Transfer Coefficients correlation formulas have been derived and compared to produce reliable mathematical models to characterize existing microchannel system. They have been applied to existing closed loop microchannel geometry with 2 *bar* pump head and 1 W/cm^2 power density. It was then possible to extract numerical predictions to size the system.
Mechanical components have been designed in order to allow performing tests on the microchannels and eventually employ them for real applications in partivle physics.

Acknowledgements

I would like to express my deep gratitude to my supervisor Marco Oriunno for his encouragement and the important technical and practical advices. In particular I am very grateful to him for having invited me to work on this project.
I would like to offer my thanks to Christopher J. Kenney, Julie Segal, Astrid Tomada and Jasmine Hasi for all the useful information that they shared with me. My thanks are also extended to Robert A. Conley and Matt McCulloch for their technical support and for their help with the experiments.

Contents

1 Introduction **4**

2 Manufacturing technique for Microchannels **5**

3 Pressure Drop Model **7**

4 Heat Transfer Model **13**

5 Application of microchannel to Particle Detectors **17**
5.1 Mechanical Stress in Michrochannels 22

6 Optimal Values **23**

7 Microchannels Systems **23**

8 Conclusion **26**

List of Figures

1 Rectangular microchannels manufactured using Bosch Process. . 5
2 Not in scale cross section of wafer showing the gap etched in the Resist, Nitride and Oxide layers. 6
3 Cross section of a microchannel manufactured employing the SLAC technique. 6
4 Choked Boundary Layer in a tube longitudinal cross section. . . 7
5 Forces acting on a circular tube. 8
6 Comparison of the Pressure Drop obtained starting from Equation 2, and Equation 9. The lines overlap. 9
7 Comparison of the Pressure Drop obtained starting from Equation 2, and Equation 9. The lines overlap. 10
8 Darcy friction coefficient variation with diameter. 12
9 Moody Diagram for a Volumetric flow rate of 2 l/min. 12
10 Variation of h, Q and Re with D. 16
11 Detail of the microchannel system analyzed. The blue arrows represent the flow direction. 18
12 Picture of the microchannel system analyzed. 18
13 Pressure drop variation with mass flow in a circular duct for a range of diameters. 20
14 Pressure drop variation with mass flow in a rectangular duct for a range of diameters. 21
15 Detail of the layers near the opening. 22
16 Diagram illustrating the disposition in parallel of the silicon wafers connected by Kapton tubing. 24
17 Cross section of the Kapton flex manifold showing the dimensions of the channels. 24
18 Drawing of a possible manifold geometry in PVC. 25
19 Drawing of the connector from different views and comparison with microchannel size. 26

List of Tables

1 Channel classification scheme [1]. 7
2 Conventional Nusselt number correlations for circular cross section. 15
3 Water properties at $20°C$. 19
4 Flow conditions for different diameter of circular channels to obtain a pressure head of $2bar$. 20
5 Flow conditions for rectangular channels of different hydraulic diameter to obtain a pressure head of $2bar$. 21
6 Maximum allowable stress before failure of the $2.3\mu m$ LTO layer. 23
7 Maximum allowable stress before failure of the $0.7\mu m$ Nitride layer. 23

1 Introduction

High heat flux removal is a major consideration in the design of a number of systems, such as Very Large Scale Integration (VLSI) chips where, according to the Moore Law, the circuitry density doubles every two years, with the temperature of the junction that must stay below the maximum rated temperature of 50^oC.
Microchannels are naturally well suited for this task, as they provide a large heat transfer surface area per unit fluid flow volume. They provide an efficient way to remove heat from a surface but pose challenges in bringing fresh coolant to the heated surface and return it to the cooling system.
Many systems developed for VLSI circuits like computer chips have been demonstrated, starting from the pioneer work of Tuckerman and Pease who employed the direct circulation of water in microchannels fabricated in silicon chips. The microchannel heat sink was able to dissipate $7.9\,MW/m^2$ with a maximum substrate temperature to inlet water temperature difference of 71^oC. However, the pressure drop was quite large at $200kPa$.

Microchannels are also of special interest for Particle Detector in High Energy Physics where material budget constraints favor integrated cooling designs that reduce the passive mass. Although the heat density is low, $< 1W/cm^2$, the sensors must be stably thermalized for the support structure and the service at sub-zero temperatures in order to reduce the unavoidably dark current of the junction. At present, the majority of the particle detectors are cooled actively with the coolant being transported through metal tubing and an interface material capable to minimize the thermal resistance between the junction and the refrigerants. Depending on the heat densities experienced by the sensors, the thermal gradient are in the range of 5 to 15 degrees. This implies also larger thermal stresses and deformations due to the mismatch of the coefficient of thermal expansion.
With microchannels, beside a lower mass design, it is possible to reduce the thermal gradients to the benefit of the thermo-mechanical stress and the dimensional stability.
Although many microchannel systems involving one single chip have been designed, those for particle detectors are made typically of several units which need to cover a large area. The large pressure drops require a special care in the design of the distribution scheme and of the interconnections, which needs to be competitive in term of low mass design with the traditional design based on metal tubing.
In this report we will describe first the existing mathematical models for the Pressure Drop and the Heat Transfer Coefficient for single phase flows in microchannels. We will apply the models to the study of the thermal performances of a single chip detector based on an alternative MEMS technique that can help to reduce costs and the material budget. Finally we will discuss a possible design for a multi sensor design like those required by the vertex detectors for the Large Hadron Collider at CERN and for the proposed International Linear

Collider.

2 Manufacturing technique for Microchannels

The Bosch process is the most commonly used and involves the cyclic use of Sulphur hexaflouride SF_6 plasma for nearly isotropic plasma etching in Silicon wafer. A passivation layer of Octafluorocyclobutane (C_4F_8) is then cyclically deposed on the substrate to protect from further etching. Ions of SF_6 on successive cycles will chemically attack the passivation layer on the bottom of the channel producing a nearly vertical structure. The depth of the etching process depends on the number of cycles. The channels are then closed by means of pyrex layer sealed on top of the silicon wafer. The result are rectangular microchannels as showed in Figure 1a and 1b.

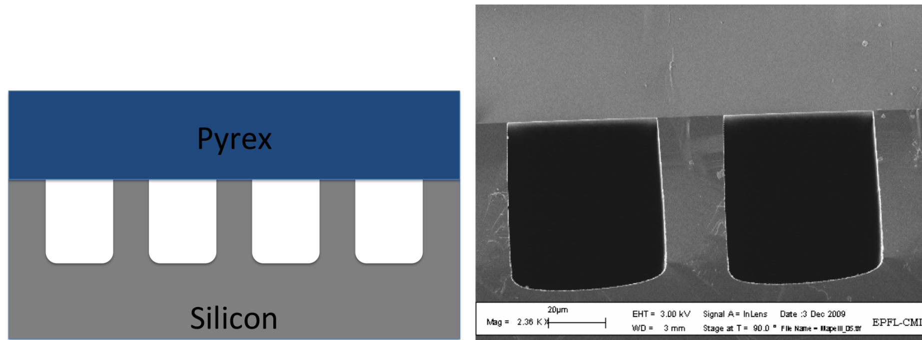

(a) Cross-section of a microchannel manufactured employing the Bosch Process.

(b) Silicon micro-channel closed with a Pyrex wafer [2].

Figure 1: Rectangular microchannels manufactured using Bosch Process.

At SLAC a new manufacturing technique was developed offering the advantage of a better budget material, hence reduced radiation length and better performance for applications in particle detectors. Microchannels are built in 4inches silicon wafers $300\mu m$ thick. The wafer is subject to chemical cleaning with Sulfuric acid and Hydrogen peroxide $(9:1)$ first and Ammonium based cleaning then. Once the wafer is perfectly clean, a $0.1\mu m$ oxide layer is grown on the surface by placing the wafer in a furnace. The same procedure is repeated to grow a $0.45\mu m$ nitride layer on top of the oxide one. At this point a $1\mu m$ layer of resist is deposed on top of the nitride layer. The microchannels geometry is then removed form the wafer exposing it for 2 seconds under UV light using a chrome mask as a stencil. After removing the excess resist, the wafer undergoes to a 2 minutes plasma etch to remove the nitride layer in the gap where the resist was removed by the UV light. The oxide layer in that gap is also removed by wet etching leaving the Silicon exposed (Figure 2).

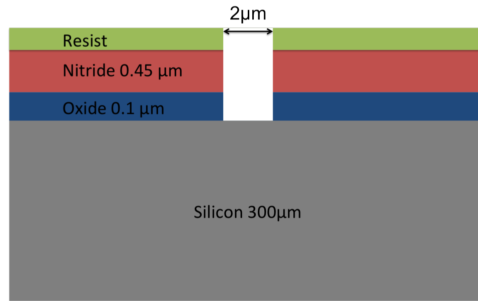

Figure 2: Not in scale cross section of wafer showing the gap etched in the Resist, Nitride and Oxide layers.

A process similar to the Bosch one is repeated to etch the actual channel in the Silicon. The difference is that only SF_6 gas is used allowing the etching to occur radially from the initiation point. The two initial cleaning stages are repeated to remove the resist layer and a $2.3\mu m$ Low Thermal-Oxide (LTO) layer is grown in the TylanBPSG furnace to seal the opening. Finally another $0.7\mu m - Si_3N_4$ is grown on top of the LTO layer to improve the mechanical strength of the system.

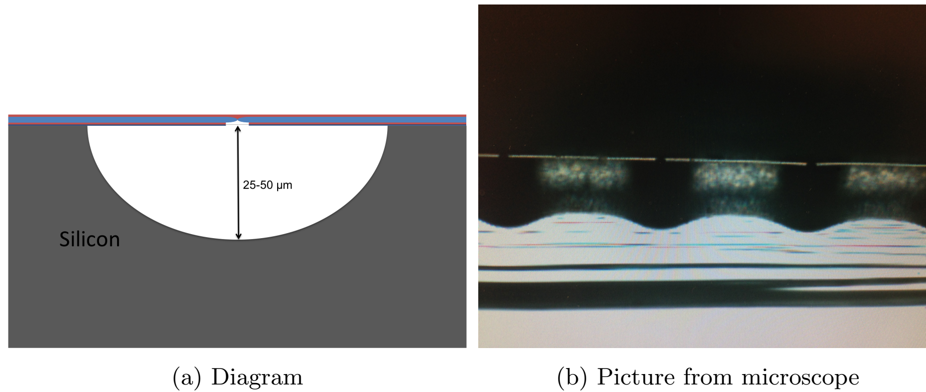

(a) Diagram (b) Picture from microscope

Figure 3: Cross section of a microchannel manufactured employing the SLAC technique.

The cross-sectional shape of the microchannels developed at SLAC is not well defined,however the is very likely to be semicircular as shown in Figure 3a. No standard correlations were produced for such not-common shape and for this reason equations for both circular and rectangular ducts are presented in Sections 3 and Section 4.
Anyone interested in pursuing this project can verify the validity of the approximation.

3 Pressure Drop Model

In order to be able to fully predict the heat transfer in microchannels it is necessary to first understand the fluidodynamics effect of a fluid flowing in small scale channels. A channel classification scheme is presented in Table 1.

Channel Classification	
Conventional Channels	$D > 3mm$
Minichannels	$3mm \geq D > 200\mu m$
Microchannels	$200\mu m \geq D > 10\mu m$
Transitional Microchannels	$10\mu m \geq D > 1\mu m$
Transitional Nanochannels	$1\mu m \geq D > 0.1\mu m$
Nanochannels	$0.1\mu m \geq D$

Table 1: Channel classification scheme [1].

An important role in internal flows is played by pressure drop ΔP along a duct length. In microchannels however viscosity plays an important role because the boundary layer thickness developed the on the wall surface is dominant and it often happens to occupy on the entire duct area with the result of a choked flow.

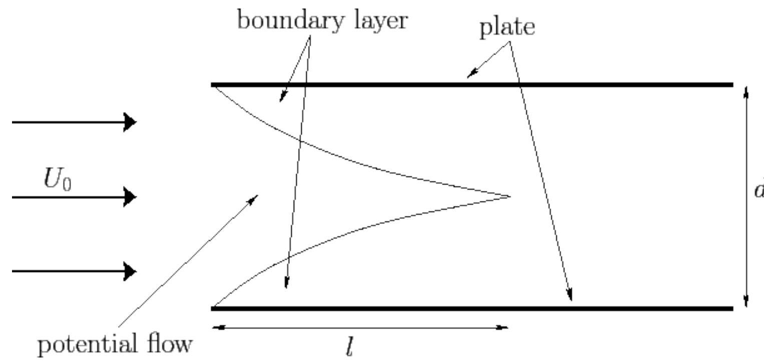

Figure 4: Choked Boundary Layer in a tube longitudinal cross section.

Circular channels

To verify the validity of different models present in literature, they have been applied on the case of channels with a circular cross-section in order to determine wether or not they lead to the same results.

Pressure difference between entry and exit of the channel must be balanced by the shear stress on the wall of the channel[3]:

$$\tau (D\pi) L = A (P_1 - P_2) \tag{1}$$

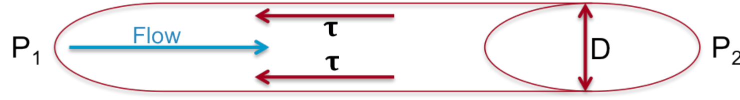

Figure 5: Forces acting on a circular tube.

D_h is the hydraulic diameter and for a circular tube $D = D_h$. L is the channel length and A is the cross sectional area. Manipulation of Equation 1 leads to:

$$\Delta P = 2\ \rho\ \frac{\tau}{\frac{1}{2}\rho v^2}\ \frac{L}{D}\bar{v}^2 = 2\ \rho\ f_F\ \frac{L}{D}\bar{v}^2 \tag{2}$$

where the Fanning friction factor for laminar flow f_F is defined as:

$$f_F = \frac{\tau}{\frac{1}{2}\rho v^2} \tag{3}$$

and:

$$f_F = \frac{Po}{Re} = \frac{16}{Re} \tag{4}$$

Where:

$$Po = f_F Re = 16 \quad \text{(theoretical value for circular cross-section)} \tag{5}$$

The flow mean velocity in the circular cross section is defined as:

$$\bar{v} = \frac{4\dot{m}}{\rho \pi D^2} \tag{6}$$

Now substituting it into the Reynolds Number for a tube of hydraulic diameter $D_h = D$ it becomes:

$$Re = \frac{\rho \bar{v} D_h}{\mu} = \frac{4\dot{m}}{\pi D \mu} \tag{7}$$

Substituting 4, 5, 6 and 7 into 2 gives:

$$\Delta P = 128\,\frac{\mu\,\dot{m}}{\rho\,\pi}\,\frac{L}{D^4} \tag{8}$$

An alternative equation is derived starting from the definition of Pressure drop by Poiseuille [4]:

$$\Delta P = Po\,\mu\,\frac{2\,v}{D_h^2}\,L \tag{9}$$

Substituting 6 into 9 and recalling that $D_h = D$ for circular ducts we get:

$$\Delta P = Po \times 2\,\frac{\mu\,\dot{m}}{\rho\,\pi}\,\frac{L}{D^4} \tag{10}$$

From 5 $Po = 16$ and Equation 10 is identical to Equations 8! The equations obtained with the two different methods are plotted on figures 6 and 7 to better

understand the pressure drop behavior. The two lines overlap confirming their equivalence.

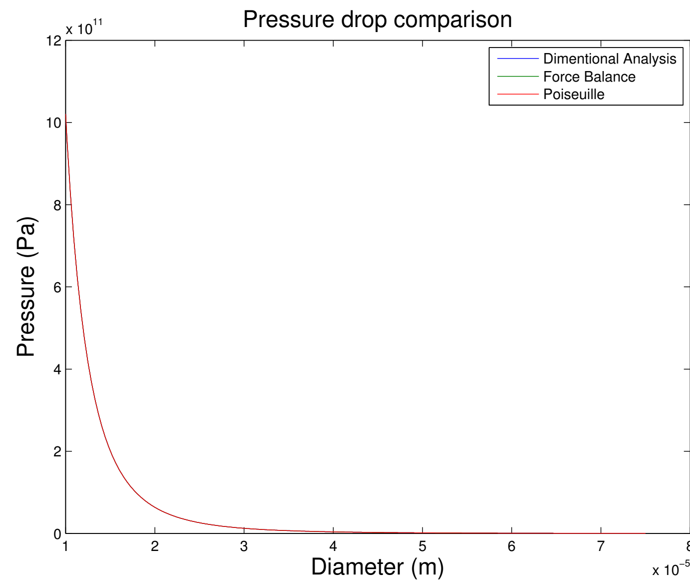

Figure 6: Comparison of the Pressure Drop obtained starting from Equation 2, and Equation 9. The lines overlap.

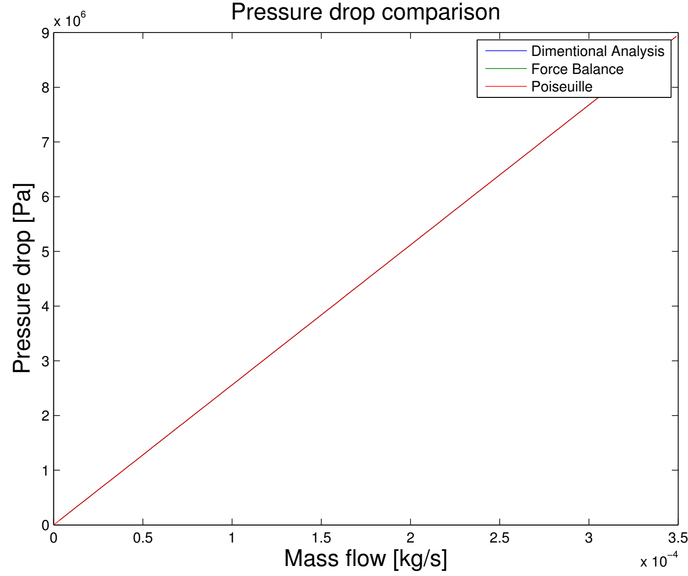

Figure 7: Comparison of the Pressure Drop obtained starting from Equation 2, and Equation 9. The lines overlap.

In Figure 6 the diameter varies from $1mm$ to $5mm$ while the volumetric flow rate is kept constant at 0.1 l/min. Same quantities are plotted in Figure 6 but varying the volumetric flow rate from 0 to 0.21 l/min and fixing the diameter to $2mm$. The Pressure drop in Figure 7 however is plotted against mass since the density is assumed to be constant and $\dot{m} = \dot{V}\rho$.
All the values are chosen to keep te the flow laminar along the whole range.

From Equation 10 it can be observed that the Pressure Drop is inversely proportional to D^4, so it reduces significantly increasing D as in Figure 6. Figure 7 shows the direct proportionality between the mass flow and the Pressure Drop. In order to reduce Pressure Drop in the system, the diameter should be chosen as large as possible and the mass flow reduced compatibly with other requirements.

Rectangular Channels

The most common correlation to determine pressure drop in rectangular channels is Equation 9, the one derived by the Poiseuille number definition. However the Poiseuille number Po is as well as the of hydraulic diameter are defined differently than from the circular cross section. Two different definitions of hydraulic diameter for rectangular geometry exist:

$$D_h = \frac{4A}{P} = 2\frac{w\,a}{w+a} \tag{11}$$

$$D_h = \sqrt{A} = \sqrt{w\,a} \tag{12}$$

Both definitions lead to the same result, however definitions of other parameters depend on the definition of hydraulic diameter that was chosen. From now on all the work will be consistent with the definition of D_h provided in Equation 12. Poiseuille number can hence be written as a function of the aspect ratio ϵ: [5]

$$Po_{\sqrt{A}} = \frac{4\pi^2\left(1+\epsilon^2\right)}{3\sqrt{\epsilon}\,(1+\epsilon)} \tag{13}$$

where:

$$\epsilon = \frac{w}{a}$$

The pressure drop is found from Equation 9. Hence substituting the value of Po relative to the aspect ratio and the mean flow velocity v as a function of mass flow:

$$v = \frac{\dot{m}}{\rho\,A} = \frac{\dot{m}}{\rho\,D_h^2}$$

the pressure drop becomes:

$$\Delta P = Po\,\mu\,\frac{2\,\dot{m}}{\rho\,D_h^4}\,L \tag{14}$$

Turbulent regime

In section 4 it will be demonstrated that turbulent flows offer better heat transfer performances than laminar flows, however for the purpose of this project, the flow is expected to constantly operate under laminar conditions to avoid undesired vibrations that could influence other measurements. A general overview of the turbulent regime predictions is covered in this section, although a detailed analysis of this phenomenon is not needed for this application.

For the case of turbulent flows, the Darcy friction factor term $f_D = 4f_F$ in the pressure drop equations presented in Section 3 assumes the form of a trascendental equation with no analytical solution [6].

$$\frac{1}{\sqrt{f_D}} = -2.0\log\left(\frac{e/D}{3.7} + \frac{2.51}{\sqrt{f_D}Re}\right) \tag{15}$$

Where e is the mean height of roughness of the pipe. A solution for f_D is found iteratively by means of the built-in function of MATLAB ”fzero”. The variation of f_D with D is showed in Figure 8.

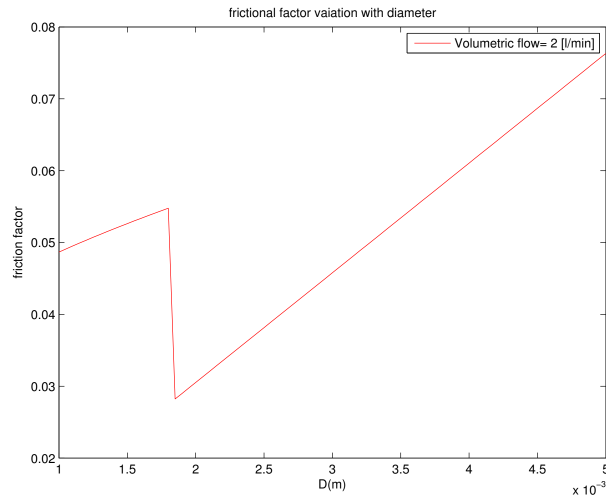

Figure 8: Darcy friction coefficient variation with diameter.

A more conventional way to plot the variation of the friction coefficient is against Reynolds Number as showed in Figure 9. This graph is usually plotted on log − log scale and is called Moody Diagram. In this case, because of shorter range of Re values, it is not convenient to visualize it on log − log scale. The values however match the ones of the original Moody Chart.

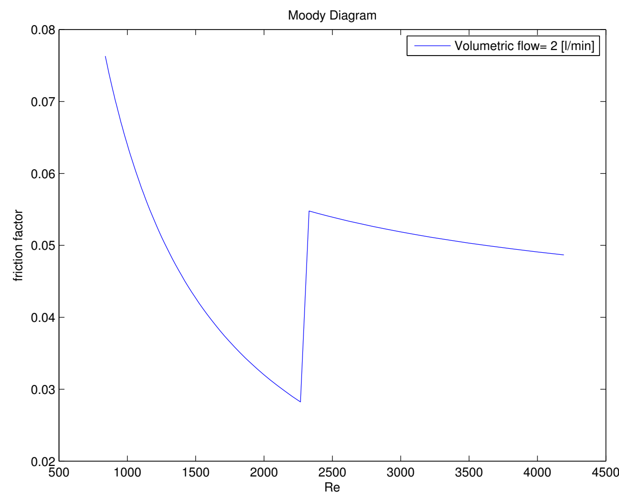

Figure 9: Moody Diagram for a Volumetric flow rate of 2 l/min.

4 Heat Transfer Model

After determining fluidodynamic behavior and predicting pressure drop, the thermodynamic part of the study is undertaken. The objective is to determine the dependence between the Convective Heat Transfer parameter h and the hydraulic diameter D_h from the definition of the Nusselt Number Nu for fully developed flows. For the sake of simplicity, only the thermal resistance inside the fluid is considered neglecting the one due to the thermal conductivity of the bulk material.

Nusselt Number is a non dimensional parameter providing a measure of the convection heat transfer occurring at the surface and depends on the channel geometry. It is defined as:

$$Nu = \frac{h\,D_h}{k} \tag{16}$$

Where k is the thermal conductivity of the fluid in the system. Rearranging Equation 16:

$$h = \frac{k}{D_h} Nu \tag{17}$$

The heat load Q in the system is a function of the convective heat transfer coefficient h:

$$Q = h\,S\,\Delta T \tag{18}$$

Where S is the wall surface across which the heat exchange occurs and is defined as:

$$S = C\,L \tag{19}$$

Where C is the section perimeter, and L is the length. ΔT is the temperature difference between the fluid and the channel's wall. The heat load can be also defined as a function of the heat flux q through a the wall surface S:

$$Q = q\,S \tag{20}$$

Now equating Equations 20 and Equation 18, and substituting 17 it comes out that:

$$\begin{aligned} Q = q\,\not{S} &= h\,\not{S}\Delta T \\ q &= h\,\Delta T \\ \frac{\Delta T}{q} = \frac{1}{h} &= \frac{D_h}{k\,Nu_C} \end{aligned} \tag{21}$$

It can be observed that the normalized thermal resistance $\frac{\Delta T}{q}$ in laminar flows is independent from the number of channels and their length, it depends on the channel diameter, duct geometry (Nu) and fluid constant of thermal conductivity of the fluid.

Theoretical prediction of Nusselt Number in microchannels is a tedious process and in literature a large number of correlations can be found. This variability of the models is due to the large number of different thermal and mechanical

assumptions that can be made as well as the effect of uncertainties of experimental measurements for such small values.

When the flow is in a laminar regime ($Re < 2300$), attention must be paid to understand wether the flow is developing or in a fully developed state. The velocity profile varies along the axial direction for a distance x after the duct entrance, this area is called Developing Length. Once the velocity profile assumes its final shape at a distance x from the channel entrance it is said to be Fully developed. The Developing length is found by means of a dimensionless distance x^+ such that:

$$x^+ = x/(D_h Re) \tag{22}$$

Same principle is valid for the temperature profile. In this case the nondimentional distance x^* is defined as:

$$x^* = x/(D_h Re Pr) \tag{23}$$

It was found experimentally that fully developed conditions occurs when x^+ and x^* are greater than 0.05.
Numerical value for the entry region length can be simply calculated from a rearrangement of Equations 22 and 23 to find x.

Nu variation in turbulent flow is described by the Dittus-Boetler equation:

$$Nu = 0.023 Re^{4/5} Pr^{\gamma} \tag{24}$$

Where Re is the Reynolds Number, Pr is the Prandtl Number and $\gamma = 0.3$ for cooling. The transition from laminar to turbulent flow is assumed at $Re \simeq 2300$.

Circular Channels

In Table 2 a number of correlations of Nusselt Number for circular cross sections Nu_C are listed together with the conditions where they apply[7].

Correlation	Flow Conditions	Range of Validity
$Nu_C = 3.66$	Fully developed	Laminar
Sieder-Tate $Nu_C = 1.86 \left(RePr\frac{D}{L}\right)^{\frac{1}{3}}$	Developing	$Re < 2200$
Stephan $Nu_C = 3.675 + \frac{0.0677\left(RePr\frac{D}{L}\right)^{1.33}}{1+0.1Pr\left(Re\frac{D}{L}\right)^{0.3}}$	Developing Constant Wall Temperature	$0.7 < Pr < 7$
Stephan $Nu_C = 4.364 + \frac{0.086\left(RePr\frac{D}{L}\right)^{1.33}}{1+0.1Pr\left(Re\frac{D}{L}\right)^{0.83}}$	Developing Constant Wall Heat Flux	$0.7 < Pr < 7$
Hausen $Nu_C = 3.66 + \frac{0.19\left(RePr\frac{D}{L}\right)^{0.8}}{1+0.117Pr\left(Re\frac{D}{L}\right)^{0.467}}$	Developing Constant Heat Flux	$Re < 2200$
Choi et al. $Nu_C = 0.000972Re^{1.17}Pr^{\frac{1}{3}}$	Developing	Laminar

Table 2: Conventional Nusselt number correlations for circular cross section.

In Figure 10 the variation of the heat transfer coefficient and heat transfer as well as the Reynolds Numebr for a constant $\Delta T = 20K$ are plotted against the diameter as defined in Equations 18, 17 and 7. Nusselt Number for laminar flow ($Re < 2300$) is assumed to be constant $Nu_C = 3.66$ as for fully developed conditions, while for turbulent regime the Dittus-Boelter equation applies. The temperature of the fluid is assumed constant along the channel since its variation is small can be neglected due to short channel length.

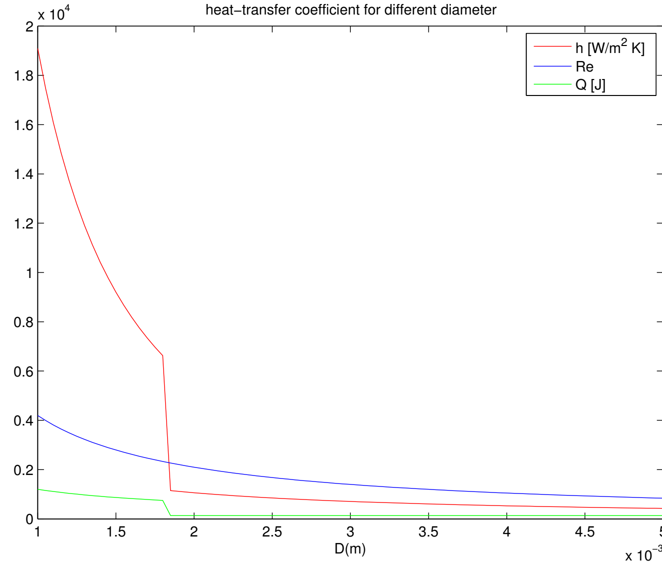

Figure 10: Variation of h, Q and Re with D.

Reynolds Number decreases as the diameter increases since, being the mass flow rate kept constant, as the diameter increases (hence the cross-sectional area), the mean flow velocity decreases. A discontinuity is observed when the flow becomes laminar at Reynolds number $Re = 2300$. Before the discontinuity, the flow is turbulent, the heat transfer coefficient h and heat load Q are higher. At this point a common mistake is to hastily conclude that smaller diameters channels are morre effective in heat transfer: In reality from small diameters a large pressure drop occurs as showed in section 3 and, as the diameter is reduced, the surface of thermal exchange is decreases too. In addition, a turbulent flow is undesirable because of the vibrations as discussed in section 3. From the plot it can also be observed that the heat load does not vary with diameter under laminar regime. Recalling that $Q = q\, S$ (20), to keep Q constant it is necessary to decrease the heat flux through the surface since the latter increases with the diameter.

Rectangular Channels

A derivation of Nusselt number similar to the one for circular channels can be conduct for rectangular cross section. Again Nu_R is constant in the fully developped laminar regime; it depends one the channel geometry and the boundary conditions. For the application presented in this report constant wall temperature and heat flux are assumed along the channel. The nusselt number can hence be derived from the following equation. A detailed study for the case of

fully-developed laminar flow is presented in reference[8].

$$Nu_R = 8.235\left(1 - 2.0421\alpha + 3.0853\alpha^2 - 2.4765\alpha^3 + 1.0578\alpha^4 - 0.1861\alpha^5\right) \tag{25}$$

Where $\alpha = \frac{1}{\epsilon}$ is the aspect ratio such that $0 < \alpha \leq 1$.

For rectangular cross section the perimeter is defined a $C = 2\,(w\,a)$. Equation 19 hence becomes:

$$S = 2\,(w + a)\;L$$

As mentioned already in Setion 3, the hydraulic diameter D_h can be defined in two ways. Although they are both valid, there is no need to develop equations based on both. Only Equation 12 will be considered from now on.

$$D_h = \sqrt{A} = \sqrt{w\,a} \tag{12}$$

Substituting D_h in Equation 21, it becomes:

$$\frac{\Delta T}{q} = \frac{\sqrt{w\,a}}{k\,Nu_R} = \frac{\sqrt{\epsilon}\,a}{k\,Nu_R} \tag{26}$$

Where the depth of the channel a is determined by the etching time.

5 Application of microchannel to Particle Detectors

Once all the mathematical models are defined, they can finally be applied on an existing microchannel geometry. The case of a 185 parallel microchannels etched in a silicon wafer is described in this section.

Figure 11 shows a drawing from Layout Editor of the geometry that is going to be studied.

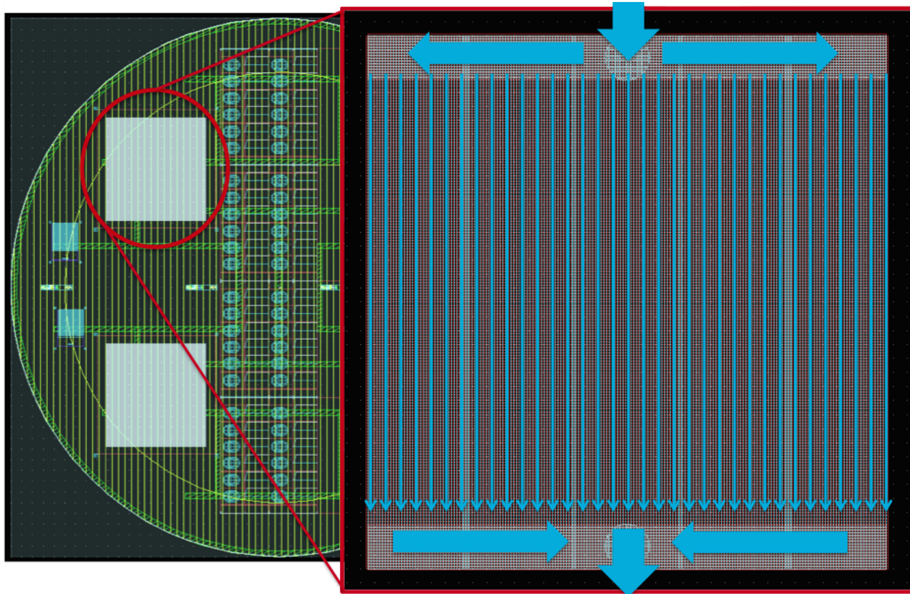

Figure 11: Detail of the microchannel system analyzed. The blue arrows represent the flow direction.

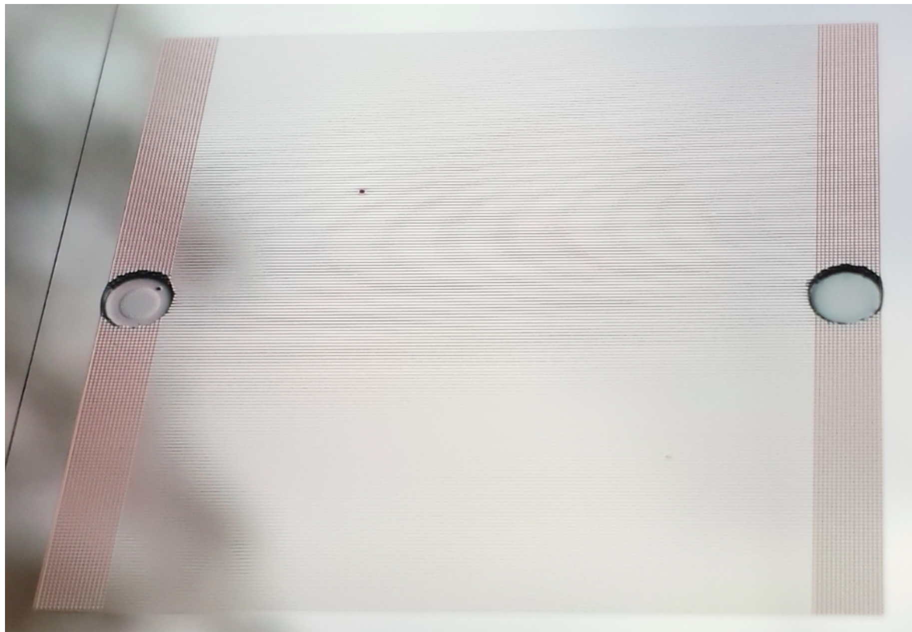

Figure 12: Picture of the microchannel system analyzed.

The 185 parallel ducts are 16 mm long and the mass flowing through them is assumed to be the same. Water is used as operating fluid with standard properties at $20°C$ as presented in Table 3. A constant Heat Flux of $1W/cm^2$ is applied through the channel walls.

Water Properties
$\rho = 997.04\ kg/m^3$
$\mu = 1.002 \times 10^{-3}\ Pa\,s$
$k = 0.58\ W/mK$
$c_P = 4181\ J/kgC$

Table 3: Water properties at $20°C$.

From Equation 22 it appears that the Non-dimensional developing length $x^+ = 0.05$ is achieved at a negligible distance x ($121\mu m$ to $7.6\mu m$) after the channel entry. For this reason the flow can be approximated to be laminar for the along the full length. The Nusselt number is hence taken as $Nu = 3.66$.
From Equation 8 the variation of Pressure Drop is plotted against the mass flow for different diameters ranging from 25 μm to 50 μm. The Diameter size might vary in the defined range depending on the etching time. For this reason different cases are proposed in this study.
The Pressure Drop obtained for the different diameters corresponds to the minimum pressure head that must be provided to keep the fluid flowing in the system. Its graphical variation can be observed in Figure 13. The horizontal line represent a constant Pressure Head of $2/, bar$, the goal is to determine the maximum mass flow that can be input into the microchannels without the pressure drop to exceed the Pressure Head limit. A value of 2 bar is taken in this case, however a more detailed analysis of the mechanicals stresses present in the system is presented in Section 5.1.
After determining the mass flow, the heat transfer performances are calculated.

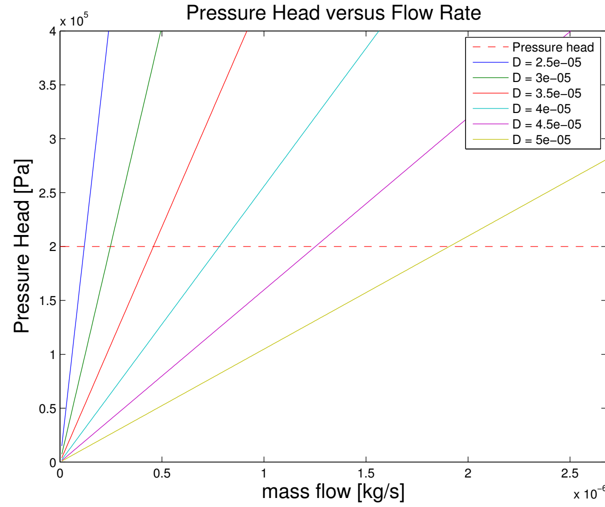

Figure 13: Pressure drop variation with mass flow in a circular duct for a range of diameters.

Diameter (μm)	Channel Mass Flow (kg/s)	Total Mass Flow (kg/s)	Reyn.	Heat Transfer Coefficient (W/m^2K)	Heat Load (W)	Temperature difference (K)
25	1.19×10^{-7}	2.21×10^{-5}	6.1	8.49×10^4	2.32	0.1178
30	2.47×10^{-7}	4.57×10^{-5}	10.5	7.08×10^4	2.79	0.1413
35	4.58×10^{-7}	8.47×10^{-5}	16.6	6.07×10^4	3.25	0.1649
40	7.82×10^{-7}	1.45×10^{-4}	24.8	5.31×10^4	3.72	0.1884
45	1.25×10^{-6}	2.32×10^{-4}	35.3	4.72×10^4	4.18	0.2120
50	1.91×10^{-6}	3.53×10^{-4}	48.5	4.25×10^4	4.65	0.2355

Table 4: Flow conditions for different diameter of circular channels to obtain a pressure head of $2bar$.

From inspection of images from the microscope, it was possible to approximate the duct geometry also as a rectangular channel with an aspect ratio $\epsilon = 4$. From Equation 13 was hence possible to determine the Poiseuille Number $Po = 22.3711$ and from Equation 25 the Nusselt number $Nu_R = 5.3327$. These constants allowed to repeat the same calculations as for the circular cross section for the same range of hydraulic diameters and pressure head of $2/, bar$. The results are showed in Figure 14 and Table 5.

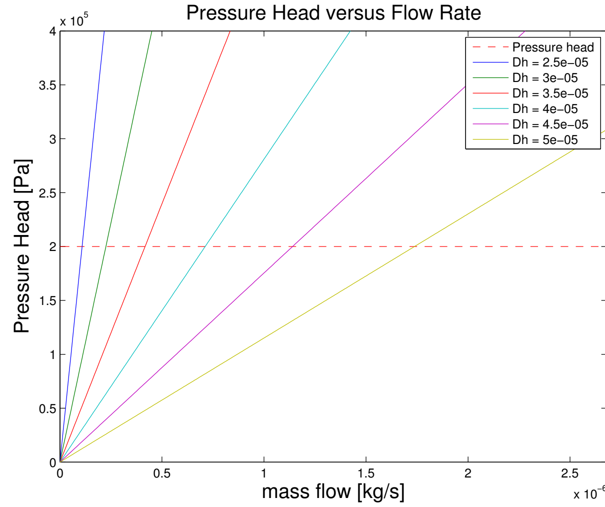

Figure 14: Pressure drop variation with mass flow in a rectangular duct for a range of diameters.

Diameter (μm)	Channel Mass Flow (kg/s)	Total Mass Flow (kg/s)	Reyn.	Heat Transfer Coefficient (W/m^2K)	Heat Load (W)	Temperature difference (K)
25	1.09×10^{-7}	2.01×10^{-5}	4.3	1.24×10^{5}	3.70	0.0808
30	2.25×10^{-7}	4.17×10^{-5}	7.5	1.03×10^{5}	4.44	0.0970
35	4.17×10^{-7}	7.72×10^{-5}	11.9	8.84×10^{4}	5.18	0.1132
40	7.12×10^{-7}	1.32×10^{-4}	17.8	7.73×10^{4}	5.92	0.1293
45	1.14×10^{-6}	2.11×10^{-4}	25.3	6.87×10^{4}	6.66	0.1455
50	1.74×10^{-6}	3.21×10^{-4}	34.7	6.19×10^{4}	7.40	0.1617

Table 5: Flow conditions for rectangular channels of different hydraulic diameter to obtain a pressure head of $2bar$.

Comparing Table 4 and 5 it can be observed that the maximum mass flow in the rectangular channel is always lower than the circular one. On the other hand the surface area of the channel of the rectangular cross section is much larger than the one of the circular duct with the same hydraulic diameter; this means a larger heat load and lower temperature difference.

The values obtained from the two different approximation differ of approximately 40% and the result for the real semicircular cross section of the microchannels is expected to lay in that range.

5.1 Mechanical Stress in Michrochannels

To determine the stresses present on the channel walls is important in order to prevent mechanical failures when pressure is applied to the system. However, due to the complexity of dicing the silicon wafer it is not possible to accurately determine the cross section shape and some assumptions must be made. The first Oxide and Nitride layers present a slot through witch the Silicon is etched as explained in Section 2. Because of this discontinuity they are assumed not to carry any load. Only the $2.3\mu m$ LTO layer and the $0.7\mu m$ Nitride layer are considered in this calculation. The cross section of the system in proximity of the opening is likely to look as showed in Figure 15.

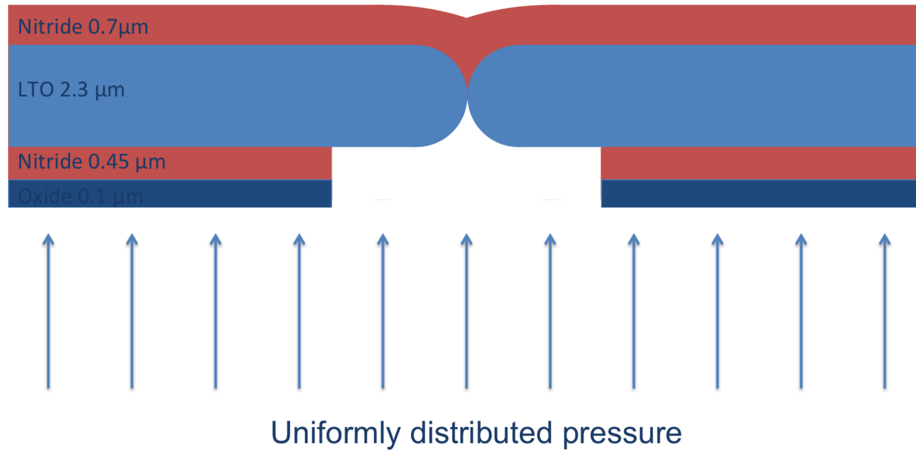

Figure 15: Detail of the layers near the opening.

The system is modeled as a classical flat rectangular plate with straight boundaries, constant thickness and uniform load over entire surface [9].The maximum pressure sustainable for an ultimate tensile strength σ_{max} in the sealing layer is:

$$P_{max} = \frac{\sigma_{max} t^2}{\beta w^2} \tag{27}$$

Where w is the width of the channel and t is the thickness on the sealing layer. For an aspect ratio $L/w \rightarrow \infty$

$$\beta = 0.5$$

Equation 27 is hence applied to both the Nitride layer and LTO layer individually for a range of widths proportional to the hydraulic diameters considered for the calculations in Section 5.

$2.3\mu m$ **LTO**	
$\sigma_{max} = 130\,MPa$	
Width (μm)	Maximum Pressure (bar)
25	22.0
30	15.3
35	11.2
40	8.60
45	6.79
50	5.50

Table 6: Maximum allowable stress before failure of the $2.3\mu m$ LTO layer.

$0.7\mu m$ **Silicon Nitride**	
$\sigma_{max} = 1\,GPa$	
Width (μm)	Maximum Pressure (bar)
25	15.7
30	10.9
35	8.00
40	6.12
45	4.84
50	3.92

Table 7: Maximum allowable stress before failure of the $0.7\mu m$ Nitride layer.

Although the Nitride layer has a much higher Ultimate Tensile Strength than the LTO, the latter is much thicker. In Equation 27 can be observed that the maximum Pressure applicable is proportional to the thickness squared, hence the LTO layer is the strongest.
In accordance with the safety factor that must be applied to the system, the maximum channel width can be taken from Table 6.

6 Optimal Values

For a pressure head of $2bar$ and a safety factor of 4 the maximum channel width is $40\mu m$ and hence $D_h = 40\mu m$ from Table 6.

From Table 4 and Table 5 a total mass flow between $1.32 \times 10^{-4}\frac{kg}{s}$ and $1.45 \times 10^{-4}\frac{kg}{s}$ can be inputted to the system with a temperature difference between the fluid and the channel walls ranging from $0.1293K$ to $0.1884K$ and absorbing an heat load between $3.72W$ and $5.92W$.

7 Microchannels Systems

Before putting the microchannels in operation it is necessary to develop the whole system of ducts, fittings and adapters to supply them with the fluid coming from a pump and a chillier located away from the particle beam. In Section 5.1 the maximum pressure that microchannels can withstand was discussed and the high pressure drop emerged from the calculations highlighted a limitation in the length and hence the impossibility of connecting them in series. It is necessity then to design an apparatus that allow their connection in parallel.
Different configurations were tried in the past with the common objective of minimising the material budget. In this chapter a new theoretical configuration is proposed. The innovation of this configuration is the presence of channels in flexible Kapton sandwiches similar to the ones widely used in flexible electronics.

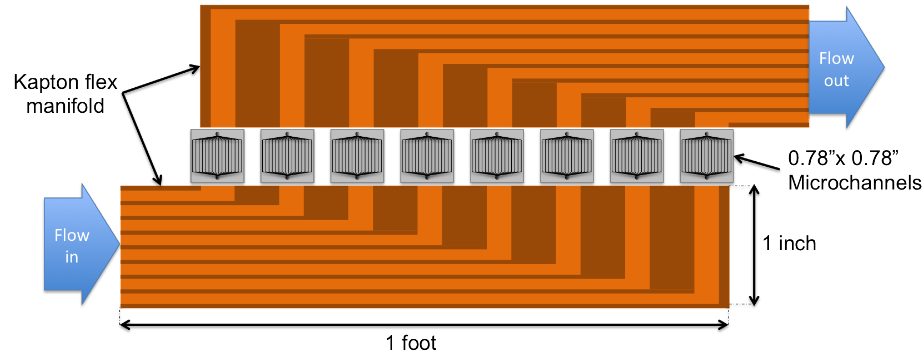

Figure 16: Diagram illustrating the disposition in parallel of the silicon wafers connected by Kapton tubing.

The advantage of this design is that Kapton has a very low radiation length, high thermal conductivity at low temperatures and is flexible. In addition the channels can be integrated with the already present Kapton circuits to further reduce the budget material. The same equations defined in Section 3 and Section 4 can be applied to determine the operation parameters.
The rectangular cross-section channels etched in Kapton are theorized having a width of $0.1\,inches$ and a height of $0.01\,inches$ as showed in Figure 17.. The hydraulic diameter is then $0.0316\,inches$ which is equivalent to $0.8\,mm$.

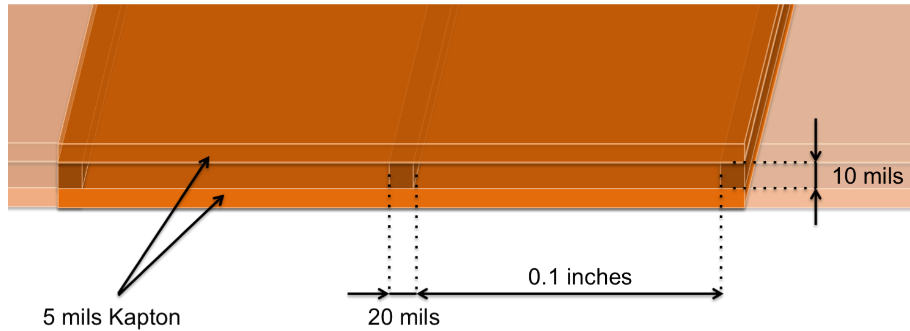

Figure 17: Cross section of the Kapton flex manifold showing the dimensions of the channels.

By inputting the dimensions of the channels into Equation 13 and Equation 14 and taking a mass flow of 1.4×10^{-4} as determined in Section 6 the pressure drop in each flexible manifold is determined as $0.061\,bar$.

Once the pressure drop in each Kapton flex manifold is determined, it is possible to do a rough estimation of the total pressure drop in the system: the fluid must be provided with a pressure sufficient to flow through the manifold, the

microchannels and then a manifold again. Hence the total pressure head that must be provided to the system is:

$$\Delta P_{total} = 0.061 + 2 + 0.061 = 2.122\,bar$$

Standard fittings for the components proposed in this project do not exist, they hence have to be designed and tested as well as the other channels. Due to the vary low thickness of the Kapton flex manifold, in a previous experiment from CERN, researchers employed a simple PVC manifold consisting of two simple plates glued together. No further details are given but they can be theorized as shown in Figure 18.

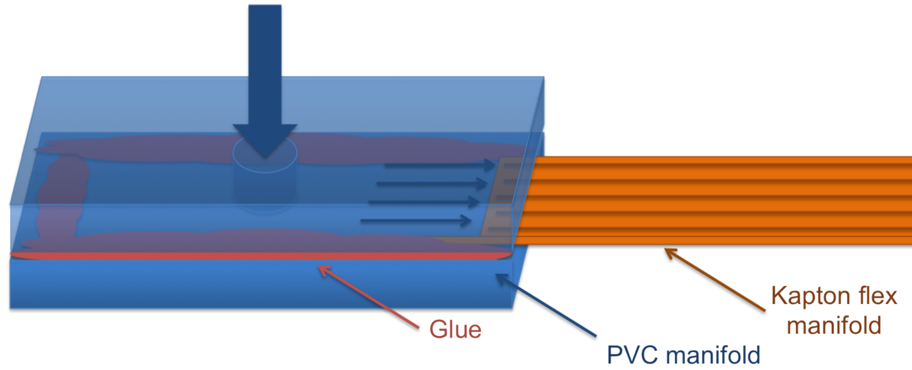

Figure 18: Drawing of a possible manifold geometry in PVC.

Another important component that was designed for this project is a connector allowing to attach a duct of larger diameter to the microchannels. A fundamental requirement for this component is the cleanliness the presence of debris might obstruct the microchannels, in addition, due to the limited dimensions it is fundamental for the object to easy to position. Because of the brittleness of the silicon wafer a snap-fit design is undesirable and due to the limited dimensions it is impossible to manufacture a thread: for this reasons the only possible solution seemed to be gluing a connector to the wafer. The design is sowed in Figure 19.

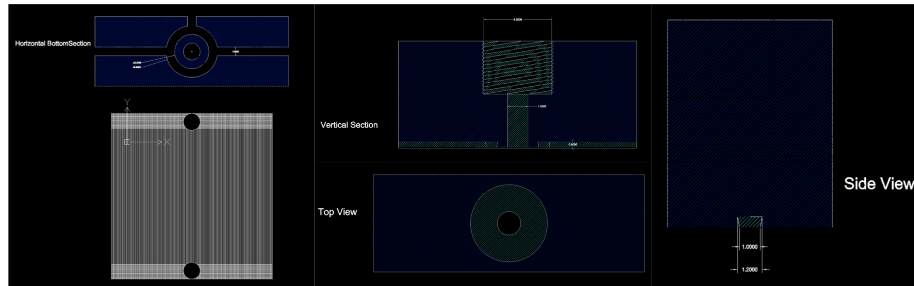

Figure 19: Drawing of the connector from different views and comparison with microchannel size.

The central hole allows aligning the connector with the hole present on the wafer by means of a Teflon guide pin. The surface of the connector is maximized to have a larger surface for the glue to stick on in order to ensure a better adhesion. The glue (epoxy) will be injected through the ducts on the bottom surface after the holes are perfectly aligned. In this way the risk of glue getting in the hole is reduced and a better alignment is guaranteed.

8 Conclusion

Microchannels are an attractive solution for cooling applications where lightweight is an important matter. In particular the technology proposed in this project is an attractive solution for particle detectors due to the low material budget and recued manufacturing cost.
Nevertheless microchannels have the limitation of the high pressure drop due to the small diameter. Theoretical predictions on the other hand show that the channel sealing layer can support the mechanical stress due to a fluid pressure of 2 *bar* with a reasonable safety margin; this solution is possible only if the microchannels are connected in parallel.
As final consideration is that the technologies described in this report offer a good compromise between the maximum pressure that microchannels can support, the low material budget and reduced manufacturing cost.

References

[1] Satish Kandlikar, Srinivas Garimella, Dongqing Li, Stephane Colin, and Michael R King. *Heat transfer and fluid flow in minichannels and microchannels*. Elsevier, 2005.

[2] A Mapelli, P. Petagna, and P. Renaud. Micro-channel cooling for high-energy physics particle detectors and electronics. In *Thermal and Thermomechanical Phenomena in Electronic Systems (ITherm), 2012 13th IEEE Intersociety Conference on*, pages 677–683, May 2012.

[3] M Bahrami, MM Yovanovich, and JR Culham. Pressure drop of fully-developed, laminar flow in microchannels of arbitrary cross-section. *Journal of fluids engineering*, 128(5):1036–1044, 2006.

[4] N Damean and PPL Regtien. Poiseuille number for the fully developed laminar flow through hexagonal ducts etched in$<$ 1 0 0$>$ silicon. *Sensors and Actuators A: Physical*, 90(1):96–101, 2001.

[5] Mohsen Akbari, David Sinton, and Majid Bahrami. Pressure drop in rectangular microchannels as compared with theory based on arbitrary cross section. *Journal of Fluids Engineering*, 131(4):041202, 2009.

[6] Edward J Shaughnessy. Introduction to fluid mechanics. 2010.

[7] Poh-Seng Lee, Suresh V Garimella, and Dong Liu. Investigation of heat transfer in rectangular microchannels. *International Journal of Heat and Mass Transfer*, 48(9):1688–1704, 2005.

[8] Satish G Kandlikar. Single-phase liquid flow in minichannels and microchannels. *Heat transfer and fluid flow in minichannels and microchannels*, pages 87–136, 2006.

[9] Warren Clarence Young and Richard Gordon Budynas. *Roark's formulas for stress and strain*, volume 7. McGraw-Hill New York, 2002.